An Investigation of Mitochondrial Inner Membranes by Rapid-Freeze Deep-Etch Techniques

Richard D. Allen, Christopher C. Schroeder, and Agnes K. Fok

Pacific Biomedical Research Center and Department of Microbiology, University of Hawaii, Honolulu 96822

Abstract. Physical fixation by rapid freezing followed by freeze-fracture and deep-etching has provided the means for potentially seeing the three-dimensional arrangement in the native state of particles on mitochondrial inner membranes. We have used these techniques to study the tubular cristae of *Paramecium* in the hope of determining the arrangement of F_1 complexes, their abundance, and location in the membranes. We also sought information regarding other respiratory complexes in these membranes. Our results, supported by stereo pairs, show that F_1 complexes are arranged as a double row of particles spaced at 12 nm along each row as a zipper following the full length of the outer curve of the helically shaped tubular cristae. There are an average of 1,500 highly ordered F_1 complexes per micrometer squared of 50-nm tubular cristae surface. The F_1 complexes definitely lie outside the membranes in their native state. Other particle subsets, also nonrandomly arrayed, were seen. One such population located along the inner helical curve consisted of large 13-nm-wide particles that were spaced at 30 nm center-to-center. Such particles, because of their large size and relative abundance when compared to F_1 units, resemble complex I of the respiratory complexes. Any models attempting to understand the coupling of respiratory complexes with F_0F_1 ATPase in *Paramecium* must take into account a relatively high degree of order and potential immobility of at least some of these integral membrane complexes.

MITOCHONDRIAL cristae are known to contain the electron transport complexes as well as the F_0F_1 ATPase complexes involved in oxidative phosphorylation. In addition, the ADP-ATP translocase, a transhydrogenase, and several less abundant integral membrane proteins reside in these membranes (6). Over 25 years ago the presence of 9-nm projections extending from these membranes into the mitochondrial matrix was discovered in beef heart muscle by Fernández-Morán (9) who used the negative-staining technique. In the ensuing years, similar globular units have been shown to be present in a wide variety of organisms across all living kingdoms of eukaryotic life (5, 26–28, 31, 35, 38). Thus it is likely that all mitochondrial cristae bear these projections. The role of the 9-nm projections was established by reconstitution studies which confirmed that the F_1 head groups represented the ATPase complexes (34).

At the same time some work was also done on estimating the relative numbers of F_0F_1 complexes per unit membrane area, e.g., Smith (38) reported that insect flight muscle has ~4,000 complexes per micrometer squared of cristae membrane, but these reports were based on use of the negative staining technique where projections can best be seen when the membranes are viewed in profile. More recent estimates of the F_1 concentrations are based on biochemical and enzymatic methods. For example, Schwerzmann et al. (42) calculated that rat liver mitochondria have 2,568 F_0F_1 complexes per micrometer squared of inner membrane.

Since the discovery of the F_0F_1 complexes at least four other complexes have been described in submitochondrial particles. Respiratory complexes II, III, and IV are smaller than F_0F_1 (complex V) and complex I is larger (16). While sheets of isolated and crystallized complexes have been extensively studied by electron microscopy (7), these complexes have yet to be identified in situ. Another question still in need of study is the topographic distribution of the F_0F_1 complexes as well as the respiratory complexes, i.e., are their distributions ordered or random. Finally, the exact vertical location of the F_0F_1 complex in native cristae is still debated from time to time (8, 26, 36), although there is persuasive evidence that they are indeed located outside the crista membrane (33) and are not induced to extrude from the membrane by the preparative methods.

With the development of new electron microscopic techniques, chemical fixatives are no longer required and cells can be physically fixed by rapid freezing. Fracturing, etching, and replication after rapid-freezing allows the observation of cellular structures in three dimensions in as nearly a native state as is currently possible to obtain. By using these techniques to reinvestigate the structure of mitochondrial cristae we hoped to show the topographical arrangement of the F_0F_1 complexes and to determine their concentration on

the membrane. We also sought morphological evidence for the arrangement of other complexes on the cristae membrane and confirmation that F_1 globules are located outside of the cristae membranes in their native state.

Using *Paramecium multimicronucleatum* we have preserved whole cells and isolated mitochondria by rapid freezing alone and have fractured these preparations and etched away the surrounding soluble phase to expose their cristae. Projections of 9-nm diameter were observed to be located entirely outside the cristae membranes. They are arranged in a nonrandom, tightly ordered pattern on these near-native tubular cristae, which were perturbed only by dehydration via sublimation at −95°C. Estimates of the membrane's area occupied by these projections and numbers per micrometers squared of membrane area and per length of tubular crista were obtained. Finally, larger 10-nm and 13 × 22-nm projections were also observed. These projections also seemed to be nonrandomly distributed.

Materials and Methods

Paramecium multimicronucleatum, growing in an axenic medium (10), was harvested at mid-log phase of growth. For comparative purposes thin-sectioned cells were prepared as previously described (2) and negatively stained mitochondrial cristae were obtained by suspending mitochondrial homogenates in phosphotungstic acid and drying on Formvar-coated grids following standard techniques (28).

Whole Cell

For observing the native structures of mitochondrial cristae, living cells or cell fractions were rapidly frozen without earlier chemical fixation or cryopreservation and then freeze-fractured, deep-etched, and replicated. For deep-etch rotary-shadowing, protocols described by Heuser (17) and Hirokawa (18) were used. Living cells were concentrated in a clinical centrifuge. A small drop of cells, still in growth medium, was placed on a thin copper mount that was designed for the Balzers freeze-etch apparatus. The mount was affixed to the plunger of a Reichert KF-80 rapid freezing device assembled for impact freezing using the MM-80 head. Cells were dropped onto a highly polished copper disk which was cooled by liquid nitrogen to −195°C. The MM-80 has a bounce-free variable force control which when optimally adjusted prevents the suspended cells from bursting on impact. Rapidly frozen cells were stored in liquid nitrogen before freeze-fracturing in a Balzers 400 apparatus. Before etching, only one pass with the microtome knife was made so that the fracture plane would be within 20 μm of the surface that impacted on the copper plate. After fracturing at −150°C, the temperature was raised to −95°C for 5–15 min for etching. Platinum to a thickness of 1.5–2 nm was evaporated onto the specimen at an angle of 24° as the specimen was being rotated. Carbon was evaporated at an angle of 80°. Replicas were cleaned in a series of bleach, chromic acid, and distilled water. The replicas were viewed in a Zeiss 10A electron microscope and stereo pairs were taken at an angle of ±10° using a rotating-tilting specimen holder. Figures illustrating this technique were printed so that regions containing evaporated platinum were light and regions lacking metal were dark.

Mitochondrial Fractions

Cells, suspended in triethanolamine-EDTA-acetic acid buffer, were broken open in a ball bearing homogenizer (Bernie-Tech Engineers, Inc., Saratoga, CA). The homogenate was centrifuged twice at 1,088 *g* for 5 min each time to remove nuclei and whole cell debris then at 3,010 *g* for two times for 10 min each to obtain an enriched mitochondria pellet. Portions of this pellet were mounted on thin copper mounts and further processed as described above for whole cells.

Results

The classical techniques of negative staining and thin-section electron microscopy demonstrated that cristae of *Paramecium*, like many other protozoa, have tubular cristae which support 9-nm projections. After negative staining the 9-nm diameter globular units were found to be aligned in a row along the outer curved margins of cristae (Fig. 1) as had previously been shown in *Tetrahymena* (26, 35) and other ciliates (5). Their center-to-center spacing was 12 nm. Such globules were not recognized along the inner curves or along straight sections of the tubules except where the tubules appeared to be distorted during isolation and drying. The extent that these projections occurred over all surfaces of the cristae could not be positively determined with this technique, since only those projections oriented in profile could be seen in a given micrograph. In thin sections of epon-embedded cells, occasional faint projections extending laterally from the cristae (Fig. 2) were observed, but these were not prominent. On the other hand, cross-sectioned cristae were more frequently observed to bear one pair of projections (Fig. 3) which, when the bend of the curved cristae could be determined, was on a curve's outer margin.

Rapid freezing followed by freeze-fracturing and deep-etching resulted in cross-fractured mitochondria which appeared to be free of the usual distortions seen in thin sections caused by the swelling or shrinking of these organelles induced by chemical fixation and dehydration. The mitochon-

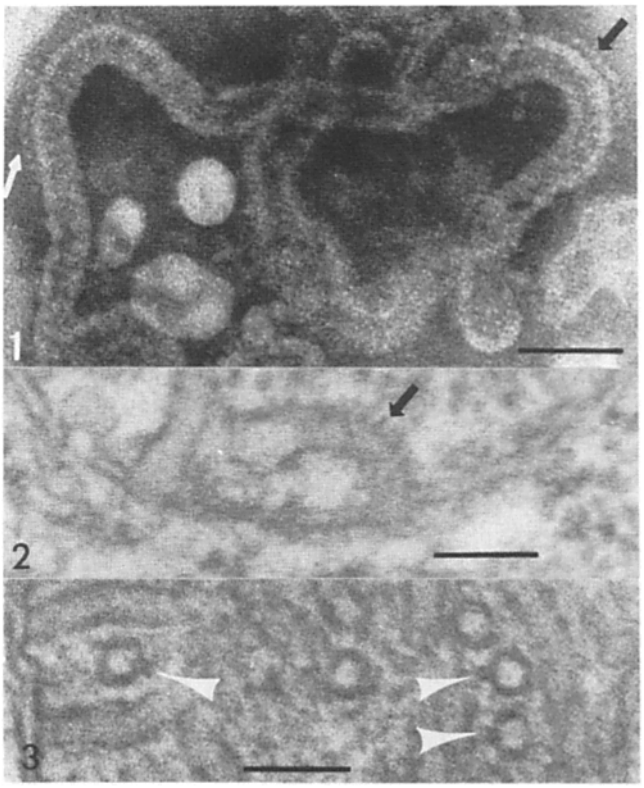

Figures 1–3. (Fig. 1) Negative-stained mitochondrial cristae fragments. Cristae of *Paramecium* are tubular and bear projections of 9-nm diameter only on their outer curved margins (*arrows*). (Fig. 2) Longitudinal section of crista in a fixed and embedded cell showing evidence of projections (*arrow*) on outer curved margin. (Fig. 3) Cross sections of 50-nm cristae each bearing one pair of projections (*arrowheads*). Bars, 0.1 μm.

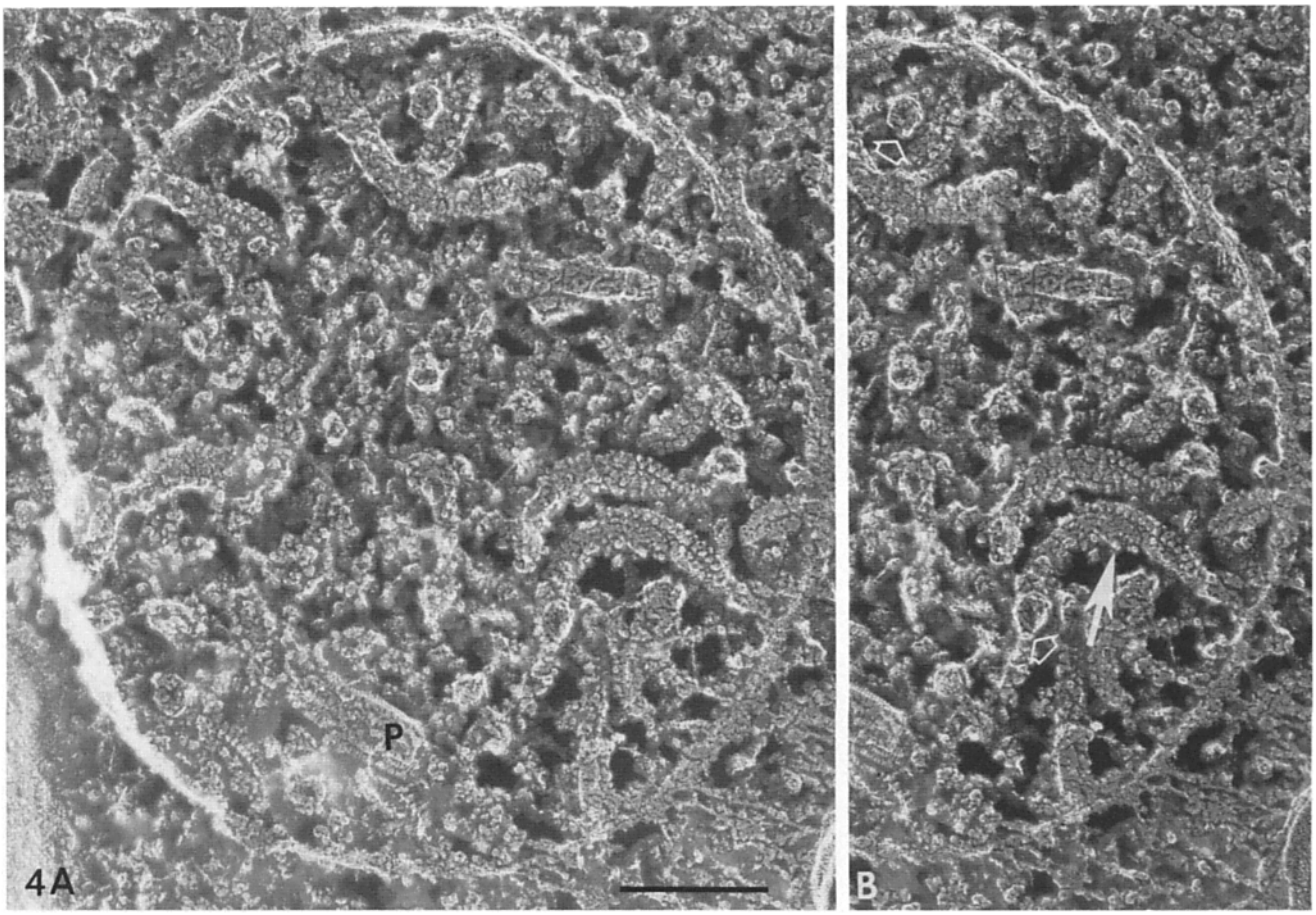

Figure 4. Mitochondrion from cryofixed whole cell (*A*) and stereo pair of right half of *A* (*B*). Tubular cristae curve in a helical pattern and bear two rows of 9-nm projections along their outer curve. Cross-fractured cristae bear one twin pair of projections (*open arrows*). A second subset of projections forming a single row follows the inner curve (*solid arrow*). The outer and inner membrane lie against each other. A paracrystal (*P*) of unknown substance is present. Bar, 0.2 μm.

drial profiles were round (Fig. 4 *A*) and the inner and outer membranes were always closely apposed to each other. The latter was true even in unetched fractures where membrane profiles could not collapse. The tubular cristae were seen both in cross fractures and oblique fractures. In stereo pairs, the tubular cristae were seen to form a shallow helix (view right side of Fig. 4, *A* and *B* with stereo viewer).

A double row of 9-nm projections was located along the outer curved margin of the helix. The remainder of the cristae surface was covered with a mosaic of irregularly shaped features which rose above the plane of the crista membrane to varying extents (*arrow*, Fig. 4 *B*). Cross-fractures of the tubular cristae had a diameter of 50 nm and contained a circular etched center of ~9–13 nm in diameter. One pair of projections could usually be detected extending into the matrix from the surface of each tubular crista (*open arrows*, Fig. 4 *B*).

Fractures of isolated whole mitochondria revealed the outer and inner membranes of mitochondria to be slightly separated after the isolation procedure (Fig. 5). As in whole cells, the tubular cristae bore rows of 9-nm-diam particles at a 12-nm center-to-center spacing. When viewed from the top of the outer curve of the helix, two rows of interdigitating particles forming a "zipperlike" arrangement (*small arrowhead*, Fig. 5) could be observed. Besides the double row of 9-nm projections, other projections of 10 nm arranged along the lateral sides of the helical cristae were sometimes observed (*arrow*, Fig. 5). Twin globular projections could be seen arising from cross-fractured cristae and continuities of the intracrista space with the intermembrane space could also be found where the cristae contacted the inner membrane (*large arrowhead*, Fig. 5 and *arrows*, Fig. 6).

Projections of various sizes could be observed extending from the surface of cross-fractured cristae. Projections that extended 7 nm from the membrane surface were frequently angular in profile with flat tops, 12 nm wide (Fig. 6).

At higher magnification and viewed from different angles, details of the twin rows of 9-nm projections could be studied. The projections, which were more or less round when viewed end on (Figs. 7 and 8), were 9–10-nm in diameter after rotary shadowing. A tiny region lacking evaporated platinum could sometimes be detected in the middle of these projections (Fig. 9). Projections were arranged in an orderly fashion in two rows, with a center-to-center spacing of 12 nm along each row. These two rows of projections were set close to each other but slightly offset which allowed the angular irregularities of the projections of one row to mesh into the notches between the projections of the second row. The over-

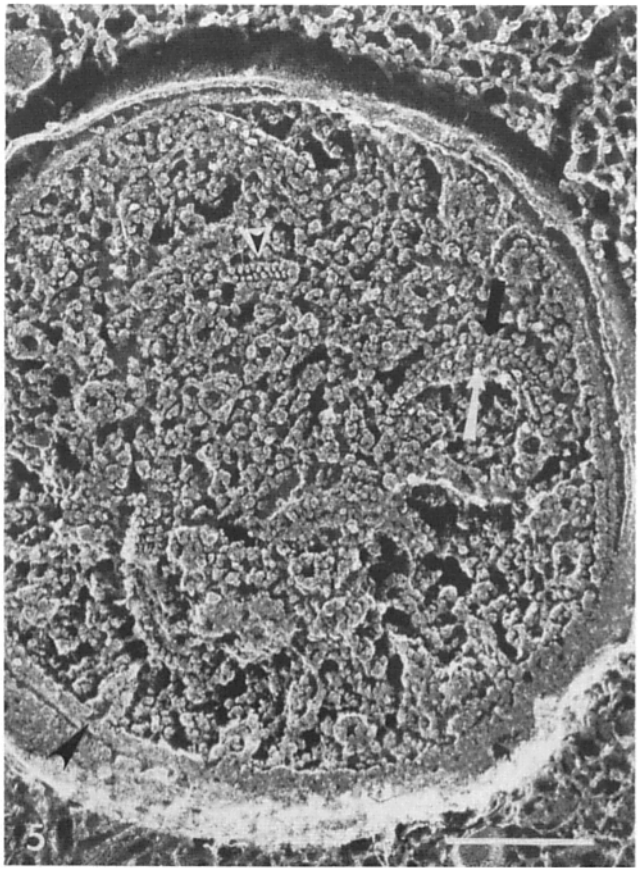

Figure 5. Mitochondrion from isolated fraction. The 9-nm projections in profile on the outer helical curve (*black arrow*) and in face view (*short arrowhead*) are seen. The outer and inner membrane are slightly separated in isolated mitochondria. A row of 10-nm particles arises from the lateral surface of the cristae indicated by the white arrow. A crista lumen opens to the intermembrane space (*long arrowhead*). Bar, 0.2 μm.

all width of the two rows was 25 nm. The height of the projections in side view was ~13.5 nm (Fig. 10), a value identical to that reported earlier for the F_1 complexes of bovine heart mitochondria (45). A distinct stalk was rarely seen, but a line indicating the absence of metal was always seen to separate the row of projections from the crista membrane (Fig. 10) in both cross-fractured and lateral views of etched cristae. There was no indication that the membranes of the cristae have fractured through a hydrophobic interior, since their projections could be viewed both face on from the top (Figs. 7 and 8) as well as projecting laterally when viewed from the sides (Fig. 10) of the helical turns of the cristae. Fracture steps indicating that one membrane leaflet of the cristae had fractured away were never seen, although these were typically found in other membranes in the same replicas.

Other projections in more or less regular arrangement were detected in situ both in whole cells and in isolated cristae. In cryofixed whole cells, indications of large particles on the inside of the helical curves were sometimes observed (*closed arrow*, Fig. 4). In isolated cristae very large particles 13 nm wide and ranging in length from 13 to 22 nm were clearly viewed aligned along the inside curve of the helix at intervals of 26–30 nm (*arrows*, Fig. 11 *A* and *B*, stereo pair), the difference in distance was probably partly a function of the amount of tilt of the helix in the region being measured. These projections protruded only 9 nm or less from the crista surface.

Discussion

That mitochondrial membranes are unique, particularly the infoldings or tubularizations of the inner membrane, is well-established both in their ultrastructure and biochemical constituents. The most prominent morphological feature of the membrane of cristae is the presence of 9-nm-diam projections which are especially clear in negative-stained preparations (e.g., reference 26). These projections are less frequently revealed by conventional thin-sectioning although they have occasionally been reported (3, 44). Rapid freezing followed by freeze substitution has recently been used to enhance their contrast in epon-embedded cells (41), but the deep-etch, rotary-shadowing technique occurring after rapid freezing has not been generally successful in showing details of these membranes in mammalian mitochondria (unpublished observations). The reason for this lack of detail for mammalian cell cristae is not clear.

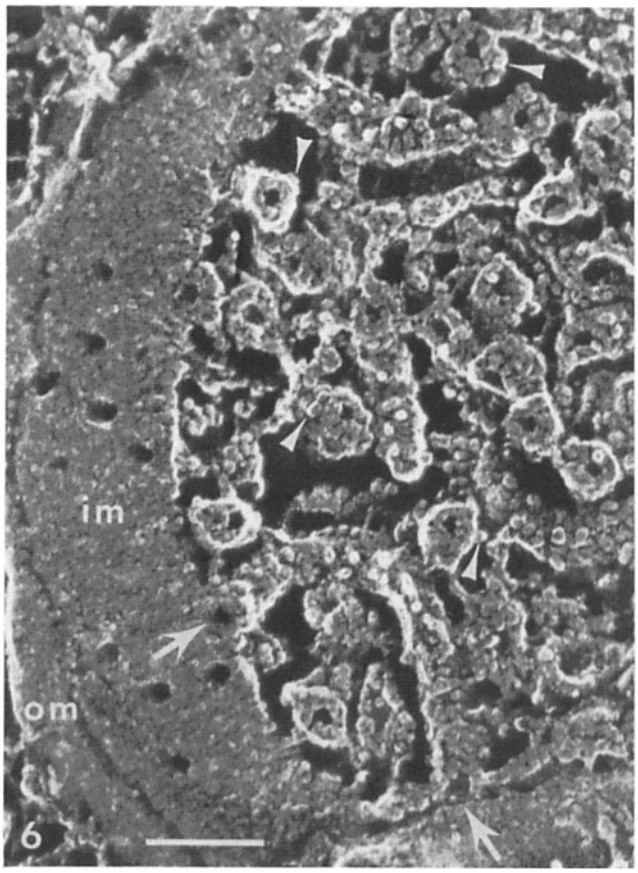

Figure 6. Tangential fracture through isolated mitochondrion exposing outer (*om*) and inner membrane (*im*) etched surfaces. One crista is connected to the inner membrane at both ends (*arrows*). This crista bears particles on its lateral and inner-curve surfaces. Many cristae are cross fractured exposing the inner lumen and laterally projecting particles of different size (*small arrowheads*). Bar, 0.1 μm.

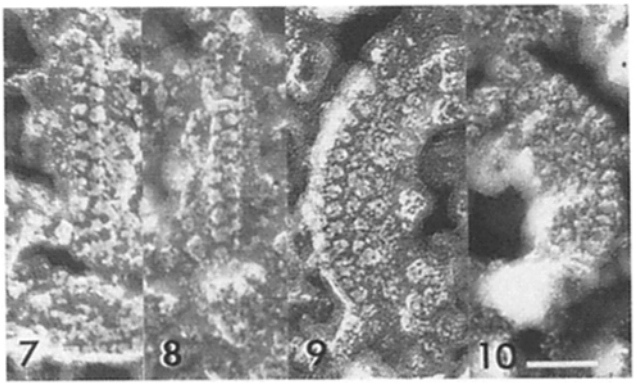

Figures 7–10. Details of the F_1 complexes viewed from the top showing staggered double rows (Figs. 7 and 8), in slightly tilted view showing one row with some central regions lacking metal (Fig. 9) and in side view (Fig. 10). Bar, 0.05 μm.

A significant finding of this study is that rapid-freezing and deep-etching has permitted us to resolve the tubular cristae of *Paramecium* as well as a number of projections which extend from cristae surfaces into the matrix. The most outstanding of these projections are the twin rows of 9-nm particles which form a zipperlike array along the outer curved margin of the helically shaped tubules. Because all visible helical segments always bear these twin rows of projections on their outer curves, we conclude that this zipper-like array extends unbroken from one end of the tubule to the opposite end as depicted in Fig. 12. A similar zipperlike array of particles has been reported in sperm, however, in this case the array was on the flagellar and not the mitochondrial membrane (11).

In addition, because these rows of 9-nm projections are identical to the images seen in negative stained preparations (see Fig. 1) and because, in other cells and tissues, identical projections have been shown to be the globular F_1 of the ATP synthase that projects into the matrix (34), we conclude that these 9-nm projections are the F_1 complexes in *Paramecium*. We also conclude that these F_1 complexes are indeed located outside the cristae membrane when fixed in their native state. Lingering doubts as to whether these complexes represent an artefact produced by the negative-staining technique can be laid to rest, at least for *Paramecium*. Although stalks were difficult to resolve, we do see evidence for these in the cleft between the 9-nm globules and the membrane.

The tightly organized and presumably immobile arrangement of these F_1 complexes was unexpected in light of some currently held views of the high fluidity of mitochondrial inner membranes and the purported ability of the inner membrane complexes to move freely within the plane of the membrane (14, 15). Although tubular cristae may represent a more basic type of cristae than their lamellaform counterparts, as has been suggested (8, 30), we propose that F_0F_1 complexes on the cristae of higher organisms should be further examined for possible heterogeneous arrangements. Of particular interest would be the arrangement of complexes on tubular cristae of the adrenal cortex and interstitial cells of the testes (29).

In fact, nonrandom arrangements of oxidative phosphorylation and respiratory complexes in mitochondria have frequently been postulated (23, 24, 32) and the kinetic evidence for such arrangements has been reviewed (21, 37, 39). The evidence for nonrandomness is particularly well-established for complexes in other energy transducing membranes, i.e., thylakoids of chloroplasts (13, 22, 40) and cyanobacteria (12, 25) and the respiratory apparatus of halophilic bacteria (22). Freeze-fracture replicas of some of these membranes have characteristic heterogenous distributions of their intramembrane particles, an organization that contributes to the efficient propagation of the photosynthetic and/or respiratory activities of these membranes and to coupling electron transport to the ATP producing complexes.

Since the F_1 complexes are packed together into rows of a constant width along the entire length of the helically wound tubule, we estimate that, for a 50-nm tubule describing a helix with a diameter of 250 nm and having a vertical spacing of 450 nm (whose matrix-facing surface area will be 0.1 μm^2 per turn), ~22% of the membrane's matrix face will be covered by this "zipper" of projections. With a constant 12-nm center-to-center spacing along each row of the double F_1 rows, one turn of a helix with the above dimensions will bear 150 F_0F_1 complexes, i.e., there will be 150 F_0F_1 complexes per 0.1 μm^2 of matrix-facing surface area. Although the projections are highly ordered there would be on average 1,500 F_0F_1 complexes for every length of tubule representing 1 μm^2 of surface area. Of course, the luminal surface area of the tubule will be much less, only 20% as much as the matrix face for the above example. We know nothing about the volume of the membrane occupied by these integral membrane complexes or the amount of luminal surface area occupied by the presumptive luminally exposed faces of these complexes. The number of F_0F_1 complexes per unit of surface area can vary with the coiling of the helix, a more tightly wound helix, one with a smaller overall diameter or shorter vertical spacing, could contain more F_0F_1 complexes per unit area than one loosely wound. Due to their arrangement on the outer curve of the helix, we conclude that the number of F_0F_1 complexes can increase without adding more membrane only by increasing the tightness of the helix or, as a result of adding more membrane, by increasing the length or number of cristae. Helical coiling of mitochondrial cristae to varying extents has been observed in *Paramecium* (1). Tighter coiling to accommodate more F_0F_1 complexes may be one means this cell uses to quickly adapt to changing requirements of energy production without necessitating new membrane production.

Mitochondrial inner membranes have long been known to be composed of a high percentage of proteins, some 70% of this membrane is composed of protein which includes, besides the F_0F_1 complexes, at least four additional well-characterized respiratory complexes (16). However, to our knowledge, the only proteins visualized in situ by the negative-staining technique have been the F_1 complexes. Tanaka (43) using a new high-resolution scanning electron-microscopic technique, has been able to visualize the matrix surface of the cristae in fractured mitochondria and has observed projections of a variety of sizes. However, no attempt to further characterize these projections has been reported. Also, this latter technique subjects the cells to a very long exposure to OsO_4, alternating with DMSO, to remove the background matrix material. How this harsh treatment

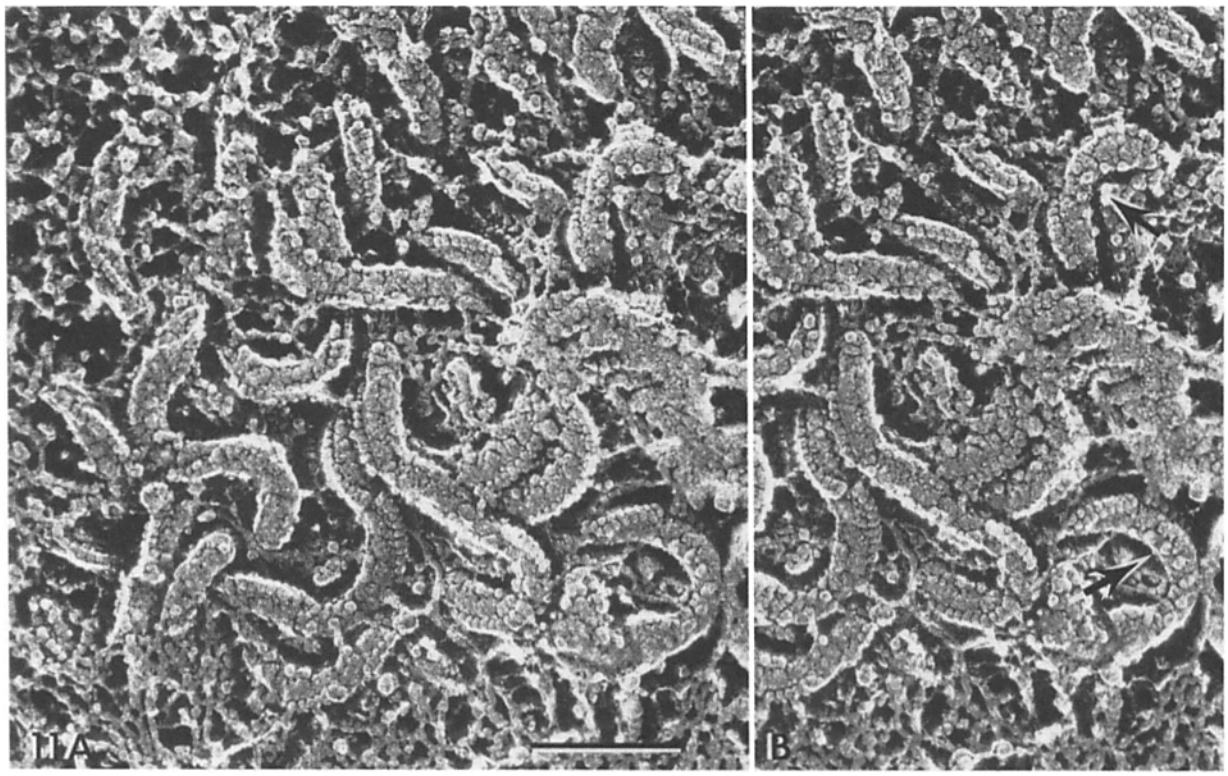

Figure 11. Stereo pair of cristae from isolated and fragmented mitochondria. Each crista bears a twin row of projections on its outer curve and a single row of large projections on its inner curve (*arrows in B*). Bar, 0.2 μm.

affects the appearance of mitochondrial membranes has not been determined.

In *Paramecium* at least two additional groups of projections of fairly distinct appearance and size protrude from the cristae into the matrix space. The first group is composed of relatively large and flat projections occurring along the inner curved margin of the helix. Though we have no biochemical or enzymic data to support the following speculation, this group of particles may be the complex I (NADH:ubiquinone oxidoreductase). Complex I is reported to be 700,000–900,000 M_r in size as compared to 500,000 M_r for the F_1 complex (16). Also in bovine heart mitochondria complex I is present in one-third to one-fifth the concentration of F_1. At a 30-nm center-to-center spacing there would be 18 of these large projections along the inside margin of one turn of a helically wound tubule having the same dimensions as that given earlier. Thus the ratio of large projections to F_0F_1 complexes would be one to eight. However, in many cases the large projections appear to be subdivided by a cleft (Fig. 11) suggesting that each elongated projection is composed of two monomers. Based on scanning transmission, electron microscopic mass determinations complex I has been determined to be a functional dimer with one flavin mononucleotide per monomer of 700-kD protein (4). The dimer makes up a unit of 1,600 kD (4). If each particle is a functional dimer, there would be 36 monomers of this type to every 150 F_0F_1 complexes giving a 1:4 ratio which is equivalent to the ratio between complex I and F_0F_1 determined by biochemical methods in beef heart (6, 16, 42).

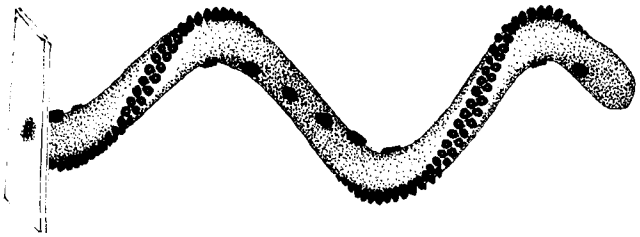

Figure 12. Drawing of one crista, roughly to scale, showing arrangement of outer twin rows of 9-nm F_1 complexes in *Paramecium* and inner single row of large 13-nm-wide particles which correspond best to complex I of the respiratory chain complexes. A third array of 10-nm particles sometimes appears on the lateral surface (not illustrated).

The second group, composed of 10-nm projections along the lateral sides of the cristae, could be either complex III (ubiquinol/ferricytochrome *c* oxidoreductase) or one of the integral membrane proteins not associated with respiration. Besides these projections the surface of the cristae is covered with a mosaic of features coated with metal. These presumably represent other peripheral or integral proteins which rise only slightly above the membrane surface. Positive identification of these regularly arranged projections as well as some of the other raised areas in the mosiac of features on the membrane surface can now be attempted on isolated cristae using the many specific antibodies that have been developed for individual polypeptides of the various complexes.

How a helically coiled tubular membrane might influence the location of integral membrane protein within that mem-

brane is an intriguing problem. Molecular shape has been used to help explain the differential partitioning of phospholipids to the two leaflets of curved membranes and to help understand why some membranes curve more than others (19, 20). Intuitively it would appear that the least amount of compression (if compression can exist in a fluid membrane) in a helically wound tubular membrane would always be on the outer curve of the helix while the most compression would occur on the inside curve. Thus, some molecular masses having certain shapes may be preferentially partitioned into regions of lesser compression. Why other complexes would preferentially align in the most compressed areas is not clear unless their shape excludes them from the less compressed regions of the membrane or they are somehow anchored to an external framework. It seems probable that intermolecular interactions between abutting F_0F_1 complexes account for the long chains of these complexes and may even account for their helical path. Specific intermolecular binding may exclude other two-dimensional arrays. Even cristae lengths could conceivably be determined by the lengths of the F_0F_1 chains themselves. However, such presumptive intermolecular forces remain to be characterized. The bases for the longer range spacing between the large complexes on the inner curve are not as easy to envision unless determined by forces outside the membrane, e.g., binding to mitochondrial matrix proteins, or by a more or less random distribution if they are allowed to move only in a back and forth path along the inner helical curve.

In summary we have shown that 9-nm projections are present on mitochondrial cristae that were physically fixed and perturbed only by sublimation at −95°C. These 9-nm projections fit the description of F_1 complexes and in *Paramecium* these F_1 complexes are highly organized and apparently immobile. There are ~1,500 of these complexes in a length of crista having a surface area of 1 μm^2. A second group of relatively large projections, also arranged in an orderly row and found on the inner helical curve conforms most closely to the size and relative abundance of complex I when compared with data on bovine heart mitochondria. There are ~18 of these large complexes (dimers?) for every 150 F_1 complexes. The third group of projections is found on the lateral side of the helix and is of unknown composition. These results show that the membranes of mitochondrial cristae, at least in some eukaryotes, have more order than some membrane fluidity studies would suggest and this order must be taken into account in developing hypotheses to explain the coupling of respiratory complexes with the F_0F_1 ATPase of these eukaryotes. These morphological studies open the way for possible immunocytochemical identification of the integral membrane proteins of cristae.

We appreciate the help of Dr. Marvin Ortel for deriving the formulas for lengths and surface areas of helically wound tubules.

This work was supported by National Science Foundation research grant DCB 85-02712, National Science Foundation instrumentation grants, and a National Institutes of Health Research Careers in Minority Institutes grant RR03061.

Received for publication 11 July 1988 and in revised form 9 February 1989.

References

1. Allen, R. D. 1988. Cytology. *In* Paramecium. H.-D. Görtz, editor. Springer-Verlag, Berlin. 4–40.
2. Allen, R. D., and A. K. Fok. 1980. Membrane recycling and endocytosis in *Paramecium* confirmed by horseradish peroxidase pulse-chase studies. *J. Cell Sci.* 45:131–145.
3. Ashhurst, D. E. 1965. Mitochondrial particles seen in sections. *J. Cell Biol.* 24:497–499.
4. Boekema, E. J., M. G. Van Heel, and E. F. J. Van Bruggen. 1984. Three-dimensional structure of bovine NADH:ubiquinone oxidoreductase of the mitochondrial respiratory chain. *Biochim. Biophys. Acta.* 787:19–26.
5. Burton, P. R. 1970. Fine structure of mitochondria of *Spirostomum ambiguum* as seen in sectioned and negatively-stained preparations. *J. Protozool.* 17:295–299.
6. Capaldi, R. A. 1982. Arrangement of proteins in the mitochondrial inner membrane. *Biochim. Biophys. Acta.* 694:291–306.
7. Costello, M. J., and T. G. Frey. 1987. Membrane proteins of the mitochondrion. *In* Electron Microscopy of Proteins. Vol. 6: Membranous Structures. J. R. Harris and R. W. Horne, editors. Academic Press Inc., London. 377–443.
8. Ernster, L., and G. Schatz. 1981. Mitochondria: a historical review. *J. Cell Biol.* 91 (suppl.):227–255s.
9. Fernández-Morán, H. 1962. Cell-membrane ultrastructure. Low-temperature electron microscopy and X-ray diffraction studies of lipoprotein components in lamellar systems. *Circulation.* 26:1039–1065.
10. Fok, A. K., and R. D. Allen. 1979. Axenic *Paramecium caudatum*. I. Mass culture and structure. *J. Protozool.* 26:463–470.
11. Friend, D. S., and J. E. Heuser. 1981. Orderly particle arrays on the mitochondrial outer membrane in rapidly-frozen sperm. *Anat. Rec.* 199: 159–175.
12. Giddings, T. H., C. Wasmann, and L. A. Staehelin. 1983. Structure of the thylakoids and envelope membranes of the cyanelles of *Cyanophora paradoxa*. *Plant Physiol. (Bethesda).* 71:409–419.
13. Gounaris, K., J. Barber, and J. L. Harwood. 1986. The thylakoid membranes of higher plant chloroplasts. *Biochem. J.* 237:313–326.
14. Hackenbrock, C. R. 1981. Lateral diffusion and electron transfer in the mitochondrial inner membrane. *Trends Biochem. Sci.* 6:151–154.
15. Hackenbrock, C. R., S. S. Gupte, and B. Chazotte. 1985. The random collision model of mitochondrial electron transport and diffusion control. *In* Achievements and Perspectives of Mitochondrial Research. Vol. 1: Bioenergetics. E. Quagliariello, E. C. Slater, F. Palmieri, C. Saccone, and A. M. Kroon, editors. Elsevier Science Publishing Co., Inc., New York. 83–101.
16. Hatefi, Y. 1985. The mitochondrial electron transport and oxidative phosphorylation system. *Annu. Rev. Biochem.* 54:1015–1069.
17. Heuser, J. E., and S. R. Salpeter. 1979. Organization of acetylcholine receptors in quick-frozen, deep-etched, and rotary-replicated *Torpedo* postsynaptic membrane. *J. Cell Biol.* 82:150–173.
18. Hirokawa, N. 1986. Quick freeze, deep etch of the cytoskeleton. *Methods Enzymol.* 134:598–613.
19. Israelachvili, J. N., S. Marcelja, and R. G. Horn. 1980. Physical principles of membrane organization. *Q. Rev. Biophys.* 13:121–200.
20. Israelachvili, J. N., D. J. Mitchell, and B. W. Ninham. 1977. Theory of self-assembly of lipid bilayers and vesicles. *Biochim. Biophys. Acta.* 470:185–201.
21. Kell, D. B., and H. V. Westerhoff. 1985. Catalytic facilitation and membrane bioenergetics. *In* Organized Multienzyme Systems: Catalytic Properties. G. R. Welch, editor. Academic Press Inc., New York. 63–139.
22. Kühlbrandt, W. 1987. Photosynthetic membranes and membrane proteins. *In* Electron Microscopy of Proteins. Vol. 6: Membranous Structures. J. R. Harris and R. W. Horne, editors. Academic Press Inc., London. 155–207.
23. Mitchell, P. 1979. Compartmentation and communication in living systems. Ligand conduction: a general catalytic principle in chemical, osmotic and chemiosmotic reaction systems. *Eur. J. Biochem.* 95:1–20.
24. Mitchell, P. 1981. Bioenergetic aspects of unity in biochemistry: evolution of the concept of ligand conduction in chemical, osmotic and chemiosmotic mechanisms. *In* Of Oxygen, Fuels and Living Matter. Part 1. G. Semenza, editor. John Wiley & Sons, New York. 1–56.
25. Mörschel, E., and E. Rhiel. 1987. Phycobilisomes and thylakoids: the light-harvesting system of cyanobacteria and red algae. *In* Electron Microscopy of Proteins. Vol. 6: Membranous Structures. J. R. Harris and R. W. Horne, editors. Academic Press Inc., London. 209–254.
26. Munn, E. A. 1974. The Structure of Mitochondria. Academic Press Inc., New York. 465 pp.
27. Oda, T., and Y. Nishi. 1963. Fundamental structure and function of mitochondrial membrane. *J. Electronmicros.* 12:290–295.
28. Parsons, D. F. 1963. Mitochondrial structure: two types of subunits on negatively stained mitochondrial membranes. *Science (Wash. DC).* 140:985–987.
29. Porter, K. R., and M. A. Bonneville. 1973. Fine Structure of Cells and Tissues. Lea and Febiger, Philadelphia.
30. Powers, E. L., C. F. Ehret, and L. E. Roth. 1955. Mitochondrial structure in *Paramecium* as revealed by electron microscopy. *Biol. Bull. (Woods Hole).* 108:182–195.
31. Prezbindowski, K. S., F. J. Ruzicka, F. F. Sun, and F. L. Crane. 1969. Membrane structure: binary membranes of mitochondrial cristae. *Exp. Cell Res.* 57:385–391.

32. Racker, E. 1970. Function and structure of the inner membrane of mitochondria and chloroplasts. *In* Membranes of Mitochondria and Chloroplasts. E. Racker, editor. Van Nostrand Reinhold Company Inc., New York. 127–171.
33. Racker, E. 1985. Reconstitutions of Transporters, Receptors, and Pathological States. Academic Press Inc., New York. 1–271.
34. Racker, E., D. D. Tyler, R. W. Estabrook, T. E. Conover, D. F. Parsons, and B. Chance. 1965. Correlations between electron-transport activity, ATP-ase, and morphology of submitochondrial particles. *In* Oxidases and Related Redox Systems. T. E. King, H. S. Mason, and M. Morrison, editors. John Wiley & Sons, New York. 1077–1101.
35. Schwab-Stey, H., D. Schwab, and W. Krebs. 1971. Electron microscopic examination of isolated mitochondria of *Tetrahymena pyriformis*. *J. Ultrastruct. Res.* 37:82–93.
36. Sjostrand, F. S. 1983. The diversity of function and structure of cellular membranes. *Subcell. Biochem.* 9:335–393.
37. Slater, E. C. 1987. The mechanism of the conservation of energy of biological oxidations. *Eur. J. Biochem.* 166:489–504.
38. Smith, D. S. 1963. The structure of flight muscle sarcosomes in the blowfly *Calliphora erythrocephala* (diptera). *J. Cell Biol.* 19:115–138.
39. Srere, P. A. 1985. Organization of proteins within the mitochondrion. *In* Organized Multienzyme Systems: Catalytic Properties. G. R. Welch, editor. Academic Press Inc., New York. 1–61.
40. Staehelin, L. A., and C. J. Arntzen. 1983. Regulation of chloroplast membrane function: protein phosphorylation changes the spatial organization of membrane components. *J. Cell Biol.* 97:1327–1337.
41. Steinbrecht, R. A. 1986. ATPase particles (portosomes) on mitochondrial cristae and the plasma membrane of an insect as demonstrated by freeze substitution. *Naturwissenschaften*. 73S:275–276.
42. Schwerzmann, K., L. M. Cruz-Orive, R. Eggman, A. Sänger, and E. R. Weibel. 1986. Molecular architecture of the inner membrane of mitochondria from rat liver: a combined biochemical and stereological study. *J. Cell Biol.* 102:97–103.
43. Tanaka, K. 1981. Demonstration of intracellular structures by high resolution scanning electron microscopy. *Scanning Electron Microsc.* 2:1–8.
44. Telford, J. N., and E. Racker. 1973. A method for increasing contrast of mitochondrial inner membrane spheres in thin sections of epon-araldite embedded tissue. *J. Cell Biol.* 57:580–586.
45. Telford, J. N., T. A. Langworthy, and E. Racker. 1984. Three proton pumps, morphology and movements. *J. Bioenerg. Biomembr.* 16:335–351.